CrossMark

J. Plasma Physics (2015), *vol.* 81, 345810302 © Cambridge University Press 2015
doi:10.1017/S0022377815000227

SSX MHD plasma wind tunnel

Michael R. Brown† and David A. Schaffner

Department of Physics and Astronomy, Swarthmore College,
500 College Ave. Swarthmore, PA 19081, USA

(Received 27 August 2014; revised 11 February 2015; accepted 12 February 2015;
first published online 17 March 2015)

A new turbulent plasma source at the Swarthmore Spheromak Experiment (SSX) facility is described. The MHD wind tunnel configuration employs a magnetized plasma gun to inject high-beta plasma into a large, well-instrumented, vacuum drift region. This provides unique laboratory conditions approaching that in the solar wind: there is no applied background magnetic field in the drift region and has no net axial magnetic flux; the plasma flow speed is on the order of the local sound speed ($M \sim 1$), so flow energy density is comparable to thermal energy density; and the ratio of thermal to magnetic pressure is of order unity (plasma $\beta \sim 1$) so thermal energy density is also comparable to magnetic energy density. Results presented here and referenced within demonstrate the new capabilities and show how the new platform is proving useful for fundamental plasma turbulence studies.

1. Introduction

Turbulence in magnetohydrodynamic (MHD) fluids is characterized by large Reynolds numbers, both fluid $R_e = Lv/\nu$ and magnetic $R_m = \mu_0 Lv/\eta$ (where ν is the plasma viscosity, and η the resistivity), and activity over a range of spatial and temporal scales (Batchelor 1970; Frisch 1995). In the solar wind, the best studied MHD turbulence laboratory (Goldstein et al. 1995; Bruno and Carbone 2013), fully-developed turbulence is observed over 4 decades in space (km to 1000's of km) and time (seconds to 1000's of seconds). In laboratory plasmas, dynamical scales are more limited (Gekelman and Stenzel 1984). In particular, the SSX MHD wind tunnel experiment displays dynamical activity over about a decade spatially (from a few cm to just a few 10's of cm) and a few decades temporally (a fraction of a μs to 10's of μs).

A hallmark of turbulence (Goldstein et al. 1995) is the spectral transfer of energy in both spatial and temporal frequencies, characterized by magnetic energy spectra $E_B(k)$ and $E_B(f)$, respectively. The typical picture of turbulent dynamics is that energy is introduced into the system at large spatial scales (i.e. low spatial frequency k) by either stirring or interaction with boundaries. Nonlinearities drive the energy to ever-smaller scales where it is ultimately dissipated as heat. This flow in k-space establishes the energy spectrum ($E_B(k)$ for magnetic fluctuations, for example). For very large systems, with a substantial separation between the injection and dissipation scales, a self-similar power-law dependence can develop in the so-called 'inertial range'.

In 3D MHD systems, turbulence subject to certain constraints can lead to the emergence of large-scale structures (Taylor 1974; Brown 1997). It can happen that quantities 'inverse-cascade' to generate self-organized, large-scale structures out of

† Email address for correspondence: doc@swarthmore.edu

https://doi.org/10.1017/S0022377815000227 Published online by Cambridge University Press

the small-scale turbulence (Frisch et al. 1975; Pouquet et al. 1976). It is also possible for turbulent magnetic energy to 'selectively decay' relative to magnetic helicity leading to the emergence of large-scale structures (Matthaeus and Montgomery 1980; Cothran et al. 2009; Gray et al. 2013). Finally, the turbulence itself can develop coherent structures related to reconnecting current sheets and intermittency (Schaffner et al. 2014b). Both energy spectra (Schaffner et al. 2014c) and structures (Schaffner et al. 2014a) can be studied in a plasma wind tunnel configuration.

In Sec. 2, we provide a machine description of the SSX MHD plasma wind tunnel. Operation and a subset of machine diagnostics are described, including new images from a fast-framing camera. In Sec. 3, we pose our major physics question: Is the statistical character of MHD turbulence universal? In Sec. 4, we share some recent results from the SSX MHD wind tunnel, including a comparison of driven versus decaying magnetic fluctuation spectra. In Sec. 5, future opportunities for an upgraded MHD wind tunnel are described.

2. Machine description: MHD plasma wind tunnel

Typical laboratory experiments exhibiting MHD turbulence feature a large applied magnetic field generated by external coils. This is particularly true of devices designed for magnetic confinement fusion (e.g. reversed field pinch (Ren et al. 2011) or tokamak (Bickerton 1997)), since a strong toroidal field is important for stability but does not participate in the dynamics. In naturally turbulent plasmas, such as the solar wind or a pulsar magnetosphere, the magnetic field is completely dynamical, meaning that the magnetic field is convected along with the plasma flow and is generated entirely from currents flowing in the plasma. In addition, natural plasmas have a wide range of plasma beta, $\beta \equiv (2\mu_0 nkT)/B^2$. The solar corona has $\beta \ll 1$, while the solar wind has $\beta \sim 1$.

In Fig. 1 we plot the operating range of the SSX MHD plasma wind tunnel, as well as some other natural and laboratory plasmas. The axes are the flow speed normalized to the Alfvén speed (i.e. the Mach Alfvén number M_{Alf}) and the thermal energy normalized to the magnetic energy (i.e. the plasma β). Natural plasmas tend to evolve to a point of equipartition of magnetic, thermal, and flow energies (i.e. both β and M_{Alf} near unity) noted by the star at the center of the figure. Most lab plasmas have a relatively high Alfvén speed because of low density and large applied magnetic field, and therefore relatively low M_{Alf}, whereas the solar wind (near Earth) is highly supersonic $M_{Alf} \cong 10$ with $\beta \sim 1$. The solar wind data presented here are from both 'slow' and 'fast' wind as measured by the Cluster spacecraft (Alexandrova et al. 2009; Sahraoui et al. 2009).

In what follows, we present a description of the SSX MHD plasma wind tunnel. The salient features are first, that the MHD wind tunnel configuration has no applied magnetic field and has no net axial magnetic flux. Second, the plasma flow speed is on the order of the local sound speed ($M \sim 1$), so flow energy is comparable to thermal energy. Third, the plasma β (ratio of thermal to magnetic pressure) is of order unity so thermal energy is comparable to magnetic energy. The first section describes the operation of the plasma source, and the second section describes diagnostic capabilities.

2.1. *Operation*

The SSX (Brown 1999) is a flexible facility used to study plasma merging, magnetic reconnection, and MHD turbulence with a variety of boundary shapes. The SSX

https://doi.org/10.1017/S0022377815000227 Published online by Cambridge University Press

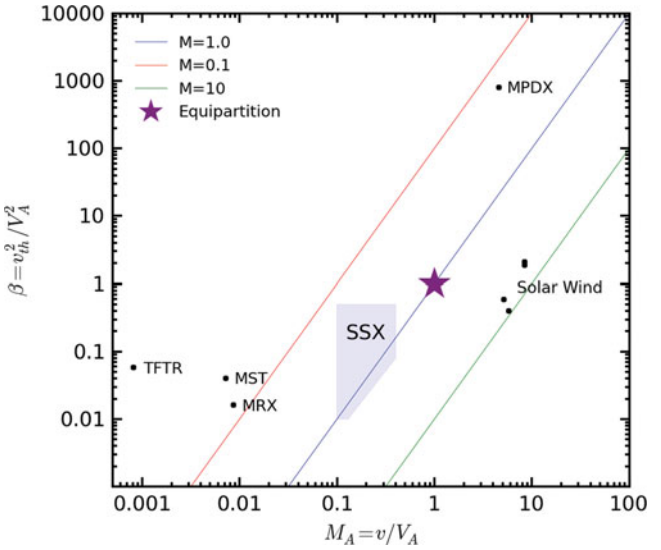


FIGURE 1. SSX plasma wind tunnel operating space (shaded region in blue). Most laboratory experiments operate in the regime of low plasma β and also at low Alfvén Mach number including tokamaks (e.g. TFTR), reverse field pinches (e.g. MST) and other laboratory astrophysics experiments (e.g. MRX) A more recent plasma dynamo experiment (MPDX) has, conversely, high Alfvén Mach number and β. The typical range of solar wind plasma is also indicated at high Alfvén Mach number and unity β. The SSX MHD wind tunnel operates closer to the point of equipartition of magnetic, thermal, and flow energies.

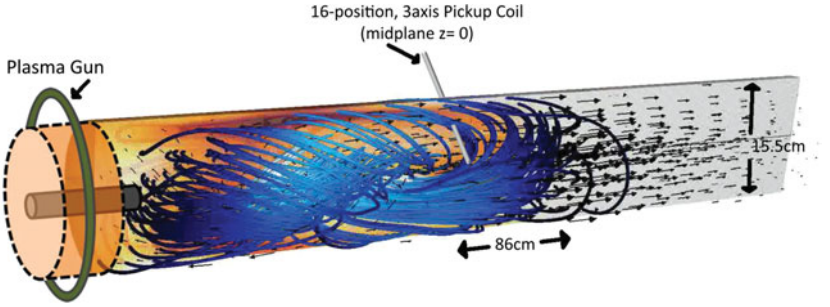


FIGURE 2. SSX plasma wind tunnel. Magnetized plasma plumes are launched by coaxial plasma guns into a flux conserving boundary. There is no applied axial magnetic field nor neutral fill gas. The image is from a simulation (Schaffner et al. 2014a). The blue lines are magnetic field lines, and the arrows are flow vectors.

device features a $L \cong 1\,\mathrm{m}$ long, high vacuum chamber in which we generate $n \leqslant 10^{21}\,\mathrm{m}^{-3}$, $T \geqslant 20\,\mathrm{eV}$, $B \leqslant 0.5\,\mathrm{T}$ hydrogen plasmas. Plasma plumes are generated by pulsed magnetized plasma guns at either end of the device. Plasmas are accelerated to high velocity ($\cong 50\,\mathrm{kms}^{-1}$) by $\mathbf{J} \times \mathbf{B}$ forces in the gun with discharge currents up to 100 kA and injected into a highly evacuated, field-free target volume called a flux conserver. The flux conserver is usually cylindrical in shape and bounded by a thick, highly conducting copper shell. In a typical experiment (Fig. 2), plasma plumes are injected at either end of a flux conserver; dynamical merging and relaxation ensue. From line-averaged measurements of n_e, T_e, T_i, and $\mathbf{B}$, we measure a plasma beta in the wind tunnel up to $\beta \sim 0.5$ (Gray et al. 2010, 2013). The line-average of $\mathbf{B}$ is constructed from 16 local measurements.

https://doi.org/10.1017/S0022377815000227 Published online by Cambridge University Press

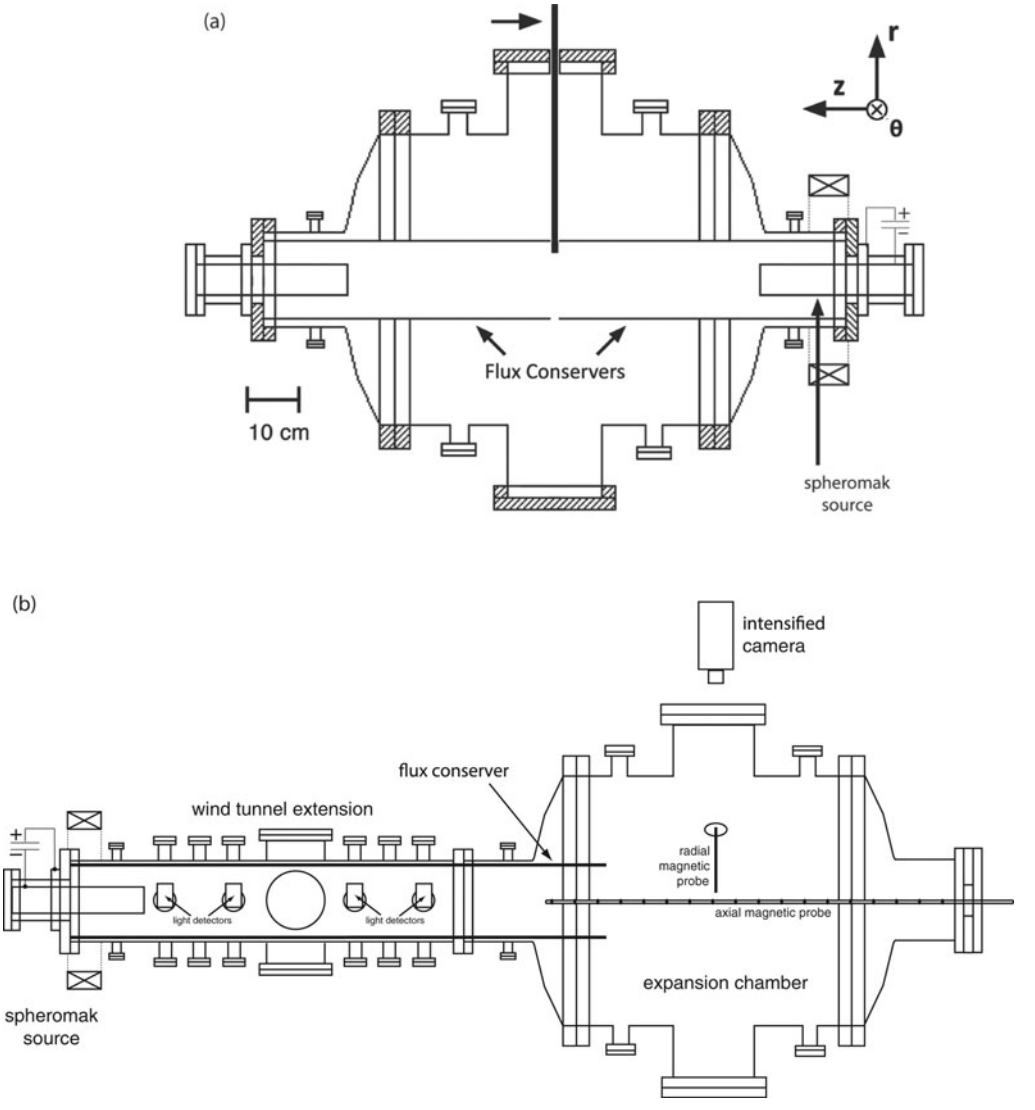


FIGURE 3. Two machine configurations for turbulence experiments: (a) Compact wind tunnel configuration with 11-1 aspect ratio. (b) Extension wind tunnel with expansion chamber configuration.

In the current configuration, we have implemented a single plasma source at one end of the high aspect ratio wind tunnel region (see Fig. 3(a)). The wind tunnel has dimensions $R = 0.08\,\mathrm{m}$ and $L = 1.0\,\mathrm{m}$ (about 20 l), but an extended length can be added as shown in Fig. 3(b). The plasma gun can inject a magnetized plasma plume of either right-handed or left-handed magnetic helicity from either end of the machine. Operationally, this means that the discharge current in the gun can be either aligned or anti-aligned with the magnetic field imbedded in the inner electrode (referred to as 'stuffing flux', Φ_{gun}, in prior work). The magnetic helicity of the plume also determines the helical pitch of magnetic field lines in the final relaxed state in the wind tunnel (Gray et al. 2013). Colliding plasma plumes have also been studied but the dynamics are much more complex.

https://doi.org/10.1017/S0022377815000227 Published online by Cambridge University Press

Plasma plumes are generated in the SSX wind tunnel by a discharge in a magnetized plasma gun. The operation is discussed in great length in the book by Bellan (2000). The gun is prepared with a fixed amount of 'stuffing flux' emanating from its end. The guns and wind tunnel are initially highly evacuated. Approximately 1 cc-atm of ultra-high purity hydrogen (a few 10^{19} atoms) is puffed into the gun and high voltage is applied. Capacitor banks for the SSX plasma wind tunnel have $C = 1.0\,\mathrm{mF}$ and can operate up to 10 kV (typically 4 kV at 8 kJ). The high voltage ionizes the gas and the subsequent high current (up to 100 kA) heats the plasma and $\mathbf{J} \times \mathbf{B}$ forces eject it out the gun. The stored magnetic energy in the plume is on the order of 1 kJ (an average field of 0.5 T in a 20 l volume corresponds to 2 kJ). The thermal and kinetic energies are less than W_{mag} since β and M_{Alf} are both less than unity.

Whether a plume of magnetized plasma emerges from the gun is a matter of pressure balance. The magnetic pressure in the gun must exceed the magnetic tension in the stuffing flux. Very approximately, if we equate the magnetic fields (Turner et al. 1983), we find

$$B_{gun} = B_{stuff} \rightarrow \frac{\mu_0 I_{gun}}{2\pi r_{gun}} = \frac{\Phi_{gun}}{\pi r_{gun}^2}$$

$$\lambda_{gun} \equiv \frac{\mu_0 I_{gun}}{\Phi_{gun}} = \frac{2}{r_{gun}}.$$

More sophisticated analysis (Geddes et al. 1998) yields a coefficient slightly different from 2, but the so-called stuffing threshold of the gun λ_{gun} is a constant of order unity (often a Bessel function zero) divided by a gun dimension (typically the radius of the inner or outer electrode).

A cryogenic pump provides the high vacuum (10^{-8} torr) for the plasma wind tunnel. The interior walls of wind tunnel are cleaned by helium glow discharge conditioning consisting of a dc discharge at 0.1 A, 400 V with about 100 mTorr of He and baking with a thermal blanket (100 °C) for several hours. In order to clean the Langmuir and Mach probes, bias is applied during He glow to collect ion current. All discharges in this study had similar external parameters: $I_{gun} = 80\,\mathrm{kA}$, $\Phi_{gun} = 1.0\,\mathrm{mWb}$, $W_{bank} = 8.0\,\mathrm{kJ}$ for the plasma source.

To add experimental flexibility, we recently mounted the SSX plasma wind tunnel (as shown in Fig. 2) onto a large expansion chamber (0.6 m diameter, 1 m long) so that we could image the emerging plasma plume with an intensified Xybion ISG-750 camera, and study turbulent statistics of the expanding plasma.

2.2. *Diagnostics*

General plasma diagnostics are discussed in textbooks (Hutchinson 2002), but diagnostics appropriate for plasma turbulence studies have particular demands. First and foremost, we require a diagnostic suite with high frequency response. The sampling frequency should be fast enough to resolve the physics of interest. The proton cyclotron frequency in a typical laboratory magnetic field of 0.1 T is 1.5 MHz. Each of the diagnostics below has frequency response of at least 1 MHz so that physics beyond the proton gyro frequency can be studied. Next, we would like the measurement to be local and non-perturbative. It is difficult to satisfy both requirements with the same diagnostic, so local probes (such as magnetic probes, Mach probes, and Langmuir probes) should be as small as possible. Non-perturbative diagnostics (such as a density interferometer, or a spectrometer) tend to provide line-averaged information. Finally, and importantly for a laboratory turbulence experiment, it is useful if turbulent quantities could be probed at multiple locations in the plasma and at high spatial

https://doi.org/10.1017/S0022377815000227 Published online by Cambridge University Press

resolution. This is a capability that is difficult in space plasmas (the tetrahedral Cluster satellite formation is the notable exception (Alexandrova et al. 2009; Sahraoui et al. 2009)), but straightforward in a laboratory.

2.2.1. *Magnetic probe array.*

Our principal measurement in the SSX MHD wind tunnel is that of magnetic fluctuations. Several aspects are critical for the design of a magnetic probe array. First, we require high spatial resolution and coverage spanning a correlation length. We also want to minimize the perturbation to the flow, so we opt for a single linear array of 16 probe triplets, separated by 4 mm. Second, we would like to maximize frequency response so we use a single turn of magnet wire for each detector (3 mm inner diameter) to minimize self-inductance, and we encase the array in a quartz jacket to ensure rapid penetration of flux. Finally, we use 65 MHz, 14 bit D-Tacq digitizers to ensure high frequency response and dynamic range. A dynamic range of 14 bits corresponds to 2^{14} or about 16 000 levels, so we can measure fields from gauss to Tesla. The typical range in the SSX plasma wind tunnel is $B = 0.1$–0.5 T. Careful calibration of the magnetic probe array is important and is described in detail in prior papers (Geddes et al. 1998; Landreman et al. 2003).

2.2.2. *Mach probe.*

Local velocity measurements are performed with a Mach probe. All of the details of construction and calibration of the SSX Mach probe appear in a prior paper (Zhang et al. 2011) (and references therein). The idea is that ion saturation current is collected on opposing faces of the probe, and the ratio of upstream to downstream currents contains information about the flow Mach number. The SSX Mach probe has a cylindrical 'Gundestrup' geometry in which six evenly spaced tungsten electrodes are encased in a boron nitride turret (Zhang et al. 2011). The component of the plasma velocity in the direction connecting the upstream and downstream faces is proportional to $\ln(J_{up}/J_{down})$. The proportionality constant is a matter of some controversy, but is of order unity. The SSX Mach probe has been calibrated *in situ* (Zhang et al. 2011). If high frequency response current transformers are used, this diagnostic can be useful at very high frequencies (over 10 MHz).

2.2.3. *He–Ne interferometer.*

The SSX plasma wind tunnel employs a He–Ne laser quadrature interferometer for measurements of line-averaged density (Buchenauer and Jacobson 1977). The technique uses a modified Mach–Zehnder configuration with a linearly polarized scene beam and a circularly polarized reference beam. The beams are de-coupled at the output using a Wollaston prism which generates signals proportional to the sine and cosine of the phase shift introduced by the plasma. The use of a circular polarizer in the reference beam effectively creates two coaxial linearly polarized beams (shifted in phase by $\pi/2$) so that the absolute phase shift due to the passage of the plasma plume can be unambiguously measured. The Wollaston prism separates the mixed circularly polarized beam into its two linearly polarized constituents (sine and cosine). The absolute phase is simply the arctan of the ratio of the signals. In a typical experiment at SSX, the scene beam passes through the plasma wind tunnel across a diameter (0.16 m), sampling plasma across a few mm wide beam. In Fig. 4, we show a time trace of the line-averaged density both for a single shot of the plasma wind tunnel and for an ensemble average, along with magnetic field (from the linear array) and Mach number (from the Mach probe).

https://doi.org/10.1017/S0022377815000227 Published online by Cambridge University Press

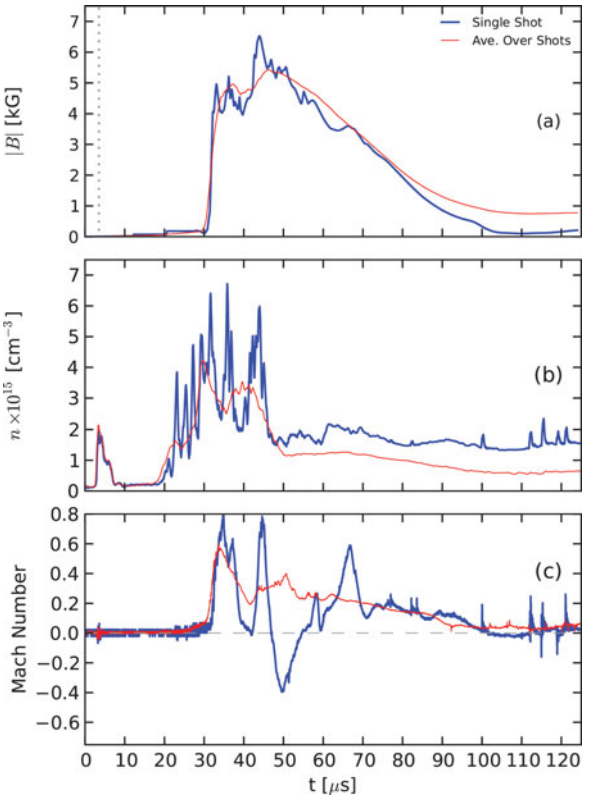


FIGURE 4. Data from a typical shot of the SSX plasma wind tunnel (blue) and ensemble average of 40 shots (red). (a) Magnetic field magnitude near the center of the device. (b) Line averaged density from the He–Ne interferometer. (c) Mach number from the Mach probe near the edge of the device.

2.2.4. *Ion Doppler spectrometer.*

In the SSX plasma wind tunnel, radial flows and ion dynamics are monitored by our ion Doppler spectroscopy system (IDS, Fig. 5) (Cothran et al. 2006). This is another example of a non-invasive diagnostic.

Impurity ions are entrained in the flow and the line-integrated motions are measured with IDS. The SSX IDS instrument measures the width and Doppler shift of either the nascent C_{III} impurity 229.7 nm line or a doped He_{II} impurity 468.6 nm line to determine the temperature and line-averaged flow velocity. The instrument (Cothran et al. 2006) employs an eschelle grating, can resolve velocity to $\leqslant 5\,\mathrm{km\,s^{-1}}$, and has an instrument temperature of 3 eV. Photon detection is via a Hamamatsu photomultiplier tube array that provides sufficient sensitivity and signal to noise ratio to resolve the full line within an MHD dynamical time (about 1 μs in SSX) for every discharge. Peak ion temperatures of 80 eV have been recorded during reconnection events as well as bi-directional outflows up to $\pm 40\,\mathrm{km\,s^{-1}}$ (Brown et al. 2012). During reconnection and merging, we measure a period of reconnection-driven ion heating with peak temperatures for carbon $T_C \cong 50\,\mathrm{eV}$ and for helium $T_{He} \cong 70\,\mathrm{eV}$ (averaged over many shots). An example of IDS data is presented in Fig. 6 to illustrate the capabilities of the diagnostic. The first three panels show radial outflows up to $50\,\mathrm{km s^{-1}}$ during a reconnection event resolved in 1 μs increments.

https://doi.org/10.1017/S0022377815000227 Published online by Cambridge University Press

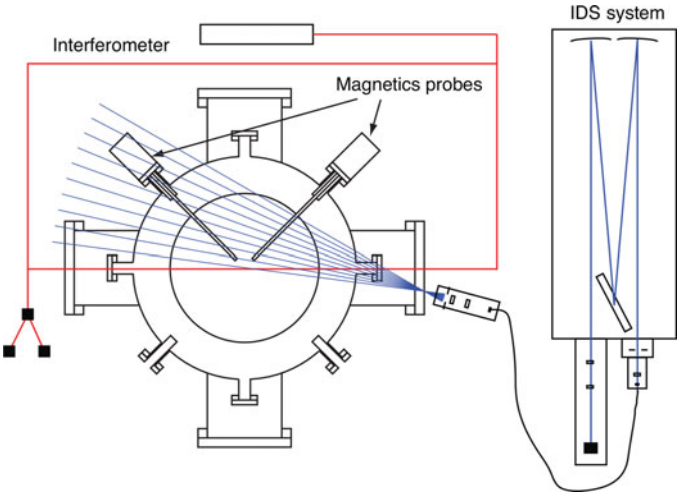


FIGURE 5. Ion Doppler spectroscopy in SSX. Cutaway end-view shows multiple chords for IDS, location of two typical magnetic probes (non-conducting quartz jacketed), and chord for He–Ne interferomenter. Our prolate 0.6 m long, 0.4 m diameter flux conserver is depicted here.

Later in the discharge, the SSX plasma has relaxed and cooled to about 8 eV. All the data are summarized in Table 1.

2.2.5. *Time of flight light detectors.*

A set of four Thorlabs Det10A silicon-biased light detectors (200–1100 nm) have been installed along the wind tunnel extension chamber at intervals of 20 cm. The recorded light traces are used to monitor the velocity of the plasma plume as it is ejected from the gun toward the expansion chamber using a time-of-flight technique. The range of velocities measured in the SSX wind tunnel is from 20 km s^{-1} to a maximum of 100 km s^{-1} with most shots falling in a range of 50–60 km s^{-1}. The system is capable of resolving velocities up to 200 km s^{-1}.

2.2.6. *Intensified camera.*

A Xybion ISG-750 intensified camera is used to capture visible spectrum images of the plasma plume as it emerges into the expansion chamber. The camera is situated approximately 50 cm above the chamber (see Fig. 3(b)) and focused on the probes in the center of the chamber. The intensifier allows exposure times to be as short as 50 ns which is necessary in order to capture the structure of plasma moving 50 km s^{-1} (or 5 cm μs^{-1}) without significant blurring; however, only a single image can be taken on each shot. Temporal evolution of the plasma is reconstructed from multiple images at different camera trigger times. The camera images thus so far have qualitatively verified the flux rope-like nature of the plasma structure. Figure 7 illustrates the typical evolution of the plasma plume in the expansion chamber. Figure 7(a) shows the plasma plume entering the field of view of the camera. The horizontal probe in view is a magnetic probe inserted coaxially with the plasma flow. It can register magnetic field direction in a vertical (y) and horizontal (x) direction (but not along the axial direction or z). Figure 7(b) shows a plume that has fully emerged and still retains its flux-rope structure. Figure 7(c) shows a point after the plume has expanded and the density dropped so no clear structures can be seen. As the plasma plume emerges from the 0.16 m diameter wind tunnel into the expansion chamber, the density drops from 10^{21} m^{-3} to 10^{20} m^{-3} or less. Only a disperse glow

https://doi.org/10.1017/S0022377815000227 Published online by Cambridge University Press

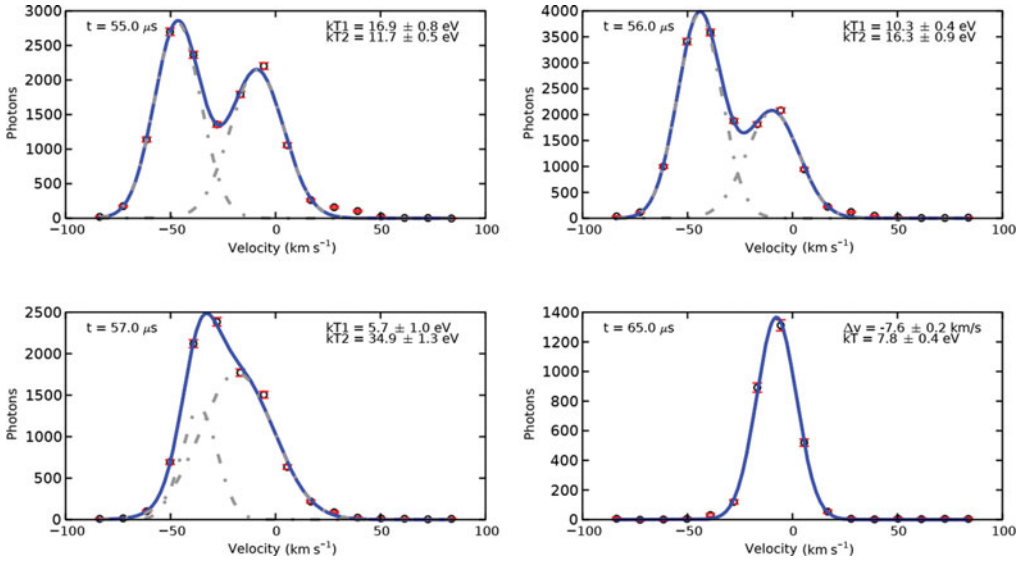


FIGURE 6. IDS data from a reconnection event in SSX. The first three panels show dynamical flows up to 50 km s^{-1} in 1 μs time increments during a reconnection event. The last panel shows a quiescent warm plasma in a relaxed state late in the discharge (8 eV).

remains, though the magnetic probes still indicate the presence of significant fields. Figures 7(d)–(f) show the magnitude of the magnetic field vector in the xy-plane for each probe channel visible in the images. The dashed vertical line indicates the timing of the above camera image with respect to the magnetic field traces. The pink line indicates the light level using the Det10A detector situated to view inside the main chamber, but out of the view of the camera (hence the slight phase difference of the light curve with respect to the magnetic field and images).

3. Major research question: universality of MHD turbulence

It is well-established that turbulence in conventional fluids like air or water has several universal statistical properties. These properties would be the same whether the turbulence was in air in a wind tunnel or in sea water in a tidal basin. It is not known whether turbulence in magnetized MHD plasma has universal statistical properties, so we ask the major research question: is the statistical character of MHD turbulence universal?

3.1. *Universality in conventional fluid turbulence*

The paradigm for fluid turbulence is the energy cascade of Kolmogorov. Fluctuation energy at different scales is represented in Fourier space as a wavenumber power spectrum, $E(k)$. The picture of the energy cascade begins with energy injected at the largest scales (smallest k) by stirring or interaction with boundaries. Nonlinearities couple energy to smaller scales (larger spatial frequency k) without dissipating energy in the process. In the inertial range, the only process at play is the transfer of energy from one wavenumber k to the next at a rate ϵ. Dissipation only occurs once the energy has been transferred to the smallest scales. According to an hypothesis by Kolmogorov (1941), the form of the wavenumber spectrum in the inertial range is

$$E(k) = C\epsilon^{2/3}k^{-5/3}.$$

https://doi.org/10.1017/S0022377815000227 Published online by Cambridge University Press

https://doi.org/10.1017/S0022377815000227 Published online by Cambridge University Press

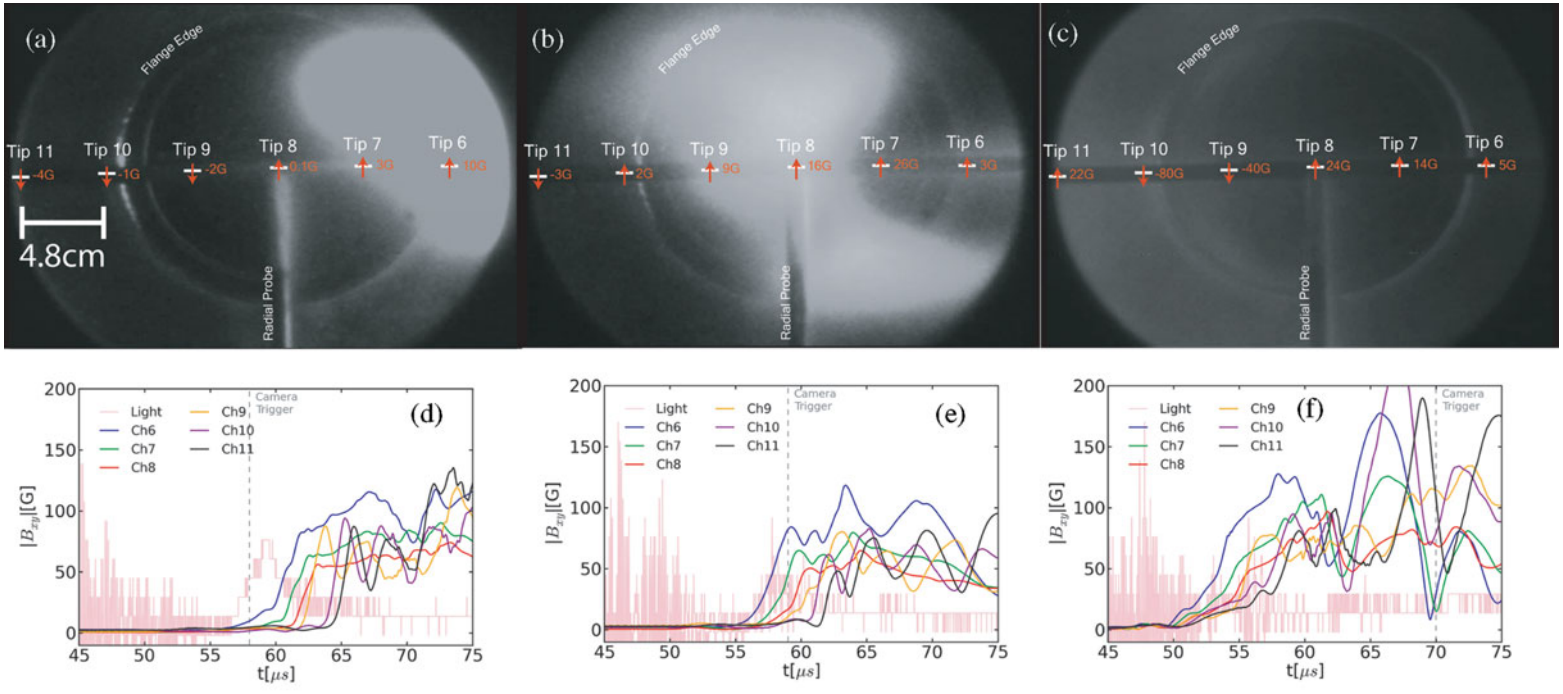


FIGURE 7. Xybion camera images at three different times in the plasma evolution. The plume is emerging from the wind tunnel on the right. It is clearly non-axisymmetric and twisted as it moves to the left. An axial magnetic probe array is depicted horizontally (channels 6–11). A radial magnetic probe array appears at the bottom of the frame. The view is down into the expansion chamber.

Parameter	High energy	Low energy
B_0	0.5 T	0.1 T
n_e	10^{15} cm^{-3}	10^{14} cm^{-3}
T_e	10 eV	20 eV
T_i	20 eV	40 eV
β	0.03	0.2
ρ_i	0.1 cm	0.6 cm
c/ω_{pi}	0.7 cm	2.3 cm
V_{Alf}	350 km s^{-1}	220 km s^{-1}
f_{ci}	7.6 MHz	1.5 MHz
R_m	150	425
S	2600	1670

Table 1. SSX MHD wind tunnel parameters.

Turbulence in magnetized plasmas is further complicated by magnetic diffusivity characterized by a second Reynolds number

$$R_m = \frac{\mu_0 v L}{\eta},$$

where η is a resistivity (typically Spitzer). Energy in turbulent magnetoplasmas can be dissipated by either viscous or resistive processes. Places in the fluid where there are sheared flows (vorticity) give rise to viscous dissipation. Places in the fluid where there are sheared magnetic fields (currents) give rise to resistive dissipation. The ratio of these two effects is given by the magnetic Prandtl number

$$Pr = \frac{R_m}{R_e} = \frac{\mu_0 \nu}{\eta}.$$

Plasmas can be dominated by either viscous or resistive dissipation. In the plasma wind tunnel described above, viscous and resistive dissipation are the same order and the magnetic Prandtl number is near unity.

3.2. *Universality in plasma turbulence*

The key reason why conventional turbulence is universal is because atoms and their interactions are truly microscopic (even 'nanoscopic' to coin a phrase). Molecular viscosity in conventional fluids allows for a single dissipation scale, and it is far removed from other dynamical scales. The wavenumber spectrum for velocity fluctuations in a conventional fluid varies as $E(k) \propto k^{-5/3}$ because the rate at which energy is transferred from one scale to the next is proportional to $v/\ell \sim kv$, so the energy transfer rate (per unit mass) is $\epsilon \sim kv^3$. In MHD turbulence, the wavenumber spectrum for magnetic fluctuations is often observed to behave the same way: $E_B(k) \propto k^{-5/3}$. This is because the rate at which magnetic energy is transferred from one scale to the next is proportional to $V_{Alf}/\ell \sim kb$, so the magnetic energy transfer rate is $\epsilon \sim kb^3$.

Universality in plasma turbulence is complicated by several factors (Alexandrova et al. 2009; Lee et al. 2010; Matthaeus and Velli 2011). Faster transfer rates are possible (due to, say whistler waves) so the spectral index for $E_B(k)$ can be steeper than 5/3 in a whistler-dominated inertial range. In addition, a plasma presents multiple pathways for dissipation at multiple scales. Molecular viscosity in conventional fluids allows for only one dissipation microscale. Plasmas can dissipate

https://doi.org/10.1017/S0022377815000227 Published online by Cambridge University Press

energy via either resistive or viscous processes. Indeed, in the solar wind, where the collisional mean free path is on the order of the Sun–Earth distance (one AU), just how energy is dissipated is a matter of some controversy. There is evidently some collision-less or wave-based dissipation mechanism at play.

If the solar wind simply expanded and cooled adiabatically, then PV^{γ} and $TV^{\gamma-1}$ would be constant. Since a spherical shell of solar wind increases in volume like r^2, then $Tr^{2(\gamma-1)}$ is also a constant for adiabatic expansion. If we use an adiabatic index of $\gamma = 5/3$, then the solar wind should cool like $T \propto r^{-4/3}$. The best fit Voyager measurements out to 20 AU shows $T \propto r^{-1/2}$ (Matthaeus and Velli 2011), so some process is heating the solar wind without inter-particle collisions. Excess magnetic energy is converted to plasma pressure increasing β towards unity. Estimates put the solar wind heating rate at 1 AU at about 1 kW per kg.

In addition to dissipation mechanisms, the combination of two possible energy injection sources can complicate the dynamics. While neutral fluid turbulence has only flow energy to initiate the cascade, MHD turbulence can be driven by either flow or magnetic energy injection, and which channel dominates can perhaps affect dynamics. Moreover, turbulent energy can transfer back and forth between magnetic field and flow. For example, there is evidence that the solar wind turbulence is primarily driven by flow energy injection which is eventually transferred into magnetic fluctuations (Roberts 2010). Similarly, turbulent magnetic spectra are observed in liquid metal experiments which have primarily flow turbulent energy (Nornberg et al. 2006). On the other hand, the energy injection source for turbulence in the SSX device is primarily magnetic (Schaffner et al. 2014c). The balance between flow-driven turbulence and magnetic-driven turbulence and its effect on turbulent characteristics such as spectra is a primary focus for forthcoming research into plasma turbulence universality on SSX as will be discussed below.

Finally, the boundary conditions on plasma turbulence can have an effect on turbulent characteristics. Again, in fluid turbulence, nanoscopic scale dissipation allows the effect of the boundary to be relatively minimized for inertial range and dissipation range effects even for relatively small systems. However, many characteristics scales that can exist in plasma turbulence (i.e. wave/instability scales, ion/electron Larmor and inertial length scales, etc.) can begin to be comparable to the size of the system. This issue can even be relevant on astrophysical scales. For example, magnetic turbulent spectra in the magnetosheath has been shown to generally be steeper than in the unbounded solar wind (Sahraoui et al. 2006; Alexandrova et al. 2008; Yordanova et al. 2008). While the reasons for this difference are still under investigation, it should be noted that the magnetosheath represents a strongly bounded plasma compared to the solar wind. In particular, the magnetic spectra observed in Yordanova et al. (2008) bear a striking resemblance to that seen on SSX (Schaffner et al. 2014c) in both spectral slope and breakpoint. Work to understand the effect of boundaries motivates the flexible configurations of SSX as well as for future larger-scale machines.

3.3. *Reconnection as an element of turbulence*

Another issue that confounds universality in plasma turbulence is that MHD turbulence can generate sites of magnetic reconnection that appear spontaneously and can be considered as an element of the turbulence itself (Servidio et al. 2011a). As the turbulence evolves, flux tubes are forced together and tangential discontinuities form at their boundaries. Local reconnection events embedded in the turbulence reveal themselves as large discontinuities in the magnetic field time series. A probability

https://doi.org/10.1017/S0022377815000227 Published online by Cambridge University Press

distribution function (PDF) of differences or increments of the magnetic field will exhibit non-Gaussian tails (Schaffner et al. 2014b).

Turbulence generates a sea of reconnection sites with a range of reconnection rates (Greco et al. 2008; Servidio et al. 2008; Greco et al. 2009; Servidio et al. 2011b). Coherent structures generated by the turbulence interact non-linearly, merge, and reconnect. Finally, the turbulence activates current sheets into a sea of reconnection sites. Active currents sheets can be patchy in space and intermittent in time. Understanding intermittency is a key aspect to the universality of plasma turbulence.

The dynamics of the turbulence can collapse tangential discontinuities in ever thinner current sheets where strong dissipation and heating can occur (Tsurutani and Smith 1979). In this scenario, the appearance of coherent structures is driven by the cascade itself. The production of ever-smaller scales in the cascade requires a topological rearrangement of fields provided by magnetic reconnection. We can study the emergence of current sheets due to *in situ* dynamics by studying the non-Gaussian statistics of PDFs of increments in the MHD plasma wind tunnel (Schaffner et al. 2014b).

4. Major results: spectra and velocity

A number of results from the compact wind tunnel configuration have already been reported. Turbulence spectra for magnetic, density and velocity fluctuations have been reported and show that magnetic fluctuation spectra have a steeper than Kolmogorov scaling (Schaffner et al. 2014a). Intermittency was also observed in the plasma and shown to increase with a decreasing analysis time window (Schaffner et al. 2014a), similar to what is observed in the solar wind (Bruno and Carbone 2013). A follow-up experiment shows that the intermittency also scaled with the amount of helicity injected by the plasma gun source and provided evidence for a relationship between this intermittency and the structure of reconnection in the plasma (Schaffner et al. 2014b). The most recent results showed the presence of anisotropy in the magnetic fluctuation spectra, again similar to observations made in the solar wind, as well as evidence for the turbulence in SSX being driven magnetic energy injection rather than flow energy (Schaffner et al. 2014c). Analysis of compact wind-tunnel data is ongoing. These initial results, however, can serve as a foundation and point of comparison for further research into the plasma universality topics discussed in the previous section. The addition of an extension tunnel with expansion chamber allows for exploration into the effect of modifying boundary conditions and flow.

In order to help add more flow energy to the plasma turbulence, a parameter scan was conducted of initial gun conditions in the extension wind tunnel with the goal of finding the maximal flow input energy to the system. Figure 8 shows the average velocity (star-marker) and standard deviation (error-bars) for plasma plumes in different initial stuffing flux and capacitor bank discharge voltages as measured using the light detectors and a time-of-flight calculation. Each marker represents an ensemble average of at least 40 discharges. In general, the plasma velocities achieved are slightly faster in this extension configuration than in the compact tunnel configuration most likely due to the increased acceleration time from the $\mathbf{J} \times \mathbf{B}$ forces of the gun (analogous to the higher speed of a cannonball out of a longer tube). However, the increased effect from the extension is moderate. Figure 8(a) does indicate that velocity increases with higher discharge voltages (which corresponds to higher peak current during the discharge and thus higher $\mathbf{J} \times \mathbf{B}$ forces in the gun).

https://doi.org/10.1017/S0022377815000227 Published online by Cambridge University Press

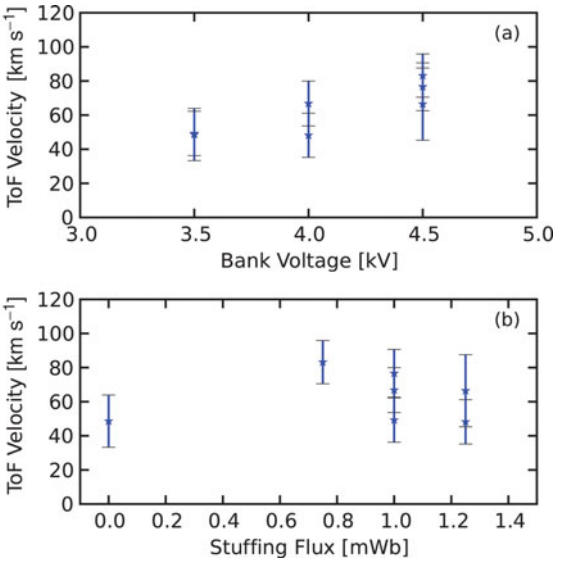


FIGURE 8. Time of flight determined plasma plume velocities as a function of (a) initial capacitor bank voltage and (b) stuffing flux. The key observation is that plume velocity is relatively insensitive to input parameters.

While pushing voltage in the bank can improve flow speeds somewhat, the maximal parameters of the bank and in particular the ignitron-switch are being reached. The other knob which can affect flow speed is the amount of stuffing flux applied to the gun. Figure 8(b) shows that peak velocities appear to be reached with moderate flux values. While some flux is necessary for the formation of the initial spheromak, too much can begin to retard the formation and the velocity of the plasma out of the gun. The results of this scan demonstrate the need for an alternate method of injected flow energy into the system and as such, a plasma accelerator design is proposed in the future opportunities section.

The effect of boundary on spectra is explored through comparison of magnetic fluctuations in the compact wind tunnel and in the expansion chamber as is shown in Fig. 9. The red curve indicates the magnetic fluctuation spectrum in the compact wind tunnel with data taken at the midplane of the tunnel as indicated by the probe position in Fig. 3(a). The spectrum has power-law behavior over approximately two decades of frequency though a breakpoint is seen near 1 MHz which likely indicates the effect of a dissipation mechanism. The magnetic fluctuation spectrum of the expansion chamber, taken using the same radial magnetic probe, but now in the middle of the expansion chamber (as indicated in Fig. 3(b)), is shown in blue. The spectrum has a peak in the power around 100 kHz which indicates that fluctuation energy has mostly settled into large-scale fluctuations by a selective decay mechanism. Below this peak, the spectrum is also power-law for approximately two decades but without a breakpoint and with a steeper slope. It should be noted that both spectra are placed arbitrarily on the y-axis with respect to one another so energy comparisons should not be made.

While some comparisons can be drawn between these two spectra regarding the effect of the boundary, a major obstacle remains in that the expansion chamber spectra are more temporally evolved and represent a decaying plasma turbulence rather than stationary turbulence. Efforts to improve the comparison are connected

https://doi.org/10.1017/S0022377815000227 Published online by Cambridge University Press

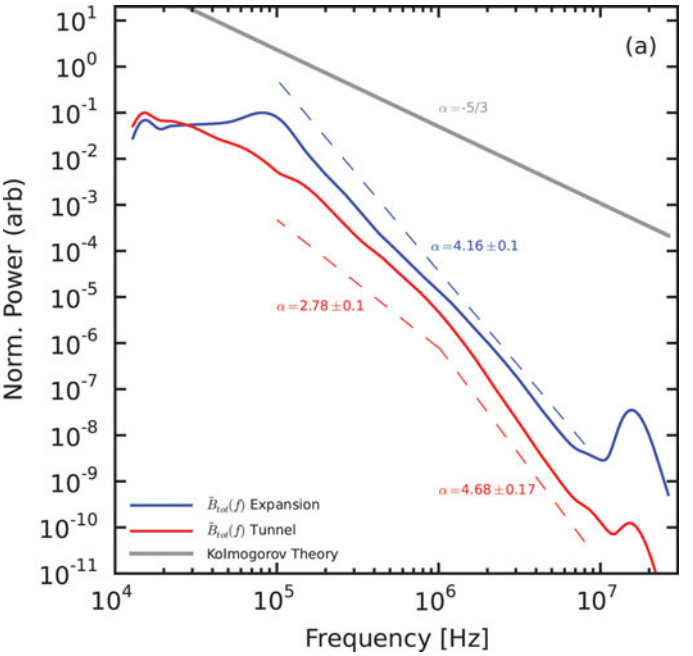


FIGURE 9. Comparison of magnetic fluctuation spectra between the compact wind tunnel and the expansion chamber.

to the need for higher velocity injection; if the spheromak plasmas can be pushed into the expansion chamber earlier, more of the stationary turbulence of the system can be observed.

Note that both experimental spectra are steeper than that predicted by Kolmogorov theory which is represented by the gray line above. The reason why the experimental magnetic fluctuation spectra are steeper is not understood and constitute a major question going forward. It is possible that the difference is due to enhanced dissipation in our experiment and/or the close proximity of the wall. We are interested in exploring similar experiments on a larger scale to study boundary effects (discussed below).

5. Future opportunities

There are at least two major opportunities that we foresee in research with high velocity MHD plasmas as discussed above. First, we have found that plasma flow speed is clamped at about $M = 1$. It would be very useful to have a mechanism to accelerate a turbulent plasma to higher flow speeds ($M \gg 1$). This would allow access to plasmas more like the solar wind as depicted in Fig. 1. Second, the SSX MHD wind tunnel has fully magnetized protons but the separation of scales is not large. We have seen that with 20 eV protons and an average field of 0.5 T, the proton gyro radius is about 0.1 cm, while the wind tunnel radius is about 8 cm, so $R/\rho_i \approx 80$. Eventually, a large-scale MHD wind tunnel with perhaps a 1 m diameter would allow for $R/\rho_i \geqslant 500$ and perhaps two decades of inertial range. In the following, we discuss these future opportunities.

https://doi.org/10.1017/S0022377815000227 Published online by Cambridge University Press

5.1. *Plasma accelerator*

The present SSX MHD wind tunnel configuration has a flow speed limited by the Alfvén speed of the plasma gun. In practice, we find the typical flow speed is a fraction of the Alfvén speed ($60\,\mathrm{km\,s^{-1}} \pm 10\,\mathrm{km\,s^{-1}}$ or $M = 0.5$). We plan to construct a multi-stage plasma accelerator to be installed in a new MHD wind tunnel extension. The idea is to pulse fast, high current theta-pinch coils sequentially behind the plasma plume. This is related to the traveling mirror concept (Bellan 1979) and to field-reversed configuration (FRC) acceleration techniques (Guo et al. 2004; Binderbauer et al. 2010). The essential physics idea is that rapidly changing magnetic flux in the pusher coil displaces trailing plasma. Magnetic pressure builds behind the plume accelerating the plasma.

Since the velocity of the plasma plume will be increased to over $100\,\mathrm{km\,s^{-1}}$ ($10\,\mathrm{cm}\mu\mathrm{s}^{-1}$), the rise time of the pusher coils needs to be on the order of 1 μs. Since the initial kinetic energy of the plume is 50–100 J, each stage of the pusher circuit should have at least 100 J of stored energy. It is not clear what the coupling efficiency will be, so we plan to over-design the pusher circuit. Our goal will be to increase the kinetic energy to 200 J (an increase of a factor of 4 in kinetic energy; doubling the flow speed). This will require 40% efficiency from the acceleration modules. Our new 65 MHz, 14-bit data acquisition system allows us to resolve temporal fluctuations down to about 1/30 μs. At flow speeds of $100\,\mathrm{km\,s^{-1}}$ ($10\,\mathrm{cm}\mu\mathrm{s}^{-1}$), we will able to resolve spatial structures on the order of 1/3 cm as they move by our probes.

The quarter-cycle rise time for the coil circuit is $\tau_{1/4} = \frac{\pi}{2}\sqrt{LC}$, where L and C are the total inductance and capacitance of the circuit. A prototype coil has an inductance of 150 nH and a vacuum feedthru adaptor, capacitor and coax add at least 100 nH. We find that in order to drop the rise time to 1 μs, the design point is forced below 10 μF for the capacitor at over 5 kV (to attain 100 J of stored energy), and a very low inductance switch such as a spark gap is required.

5.2. *Intermediate scale MHD wind tunnel*

We suggest that an interesting laboratory plasma facility would be an intermediate scale magnetized plasma wind tunnel with length about 10 m and diameter 1 m. Our experience suggests that with large-scale fields of 1000 gauss and plasma temperatures of 10's of eV, the dissipation scale would be less than 1 cm while the energy injection scale would be about 1 m, providing two full decades of scale separation. The scale of the device would be approximately that of the LAPD device at UCLA. A key difference is that the MHD wind tunnel would be pulsed from a high flux, high energy source. The plasma source would be similar to that of the now closed SSPX spheromak device previously operated at LLNL (Hooper et al. 2012).

We envision that the vacuum chamber would consist of up to 10 48-inch long, 48-inch diameter sections as illustrated in Figure 10. The plasma-facing material would be highly conducting copper perhaps 0.25 inch thick wall, 1 m diameter, and 10 m long. This is 4800 pounds of copper. We have found that it is critical to bake and plasma-clean the flux-conserving boundaries in vacuum. Copper (or a tungsten coating) can adsorb up to 10^{20} H_2 molecules per square meter on its surface. A high velocity MHD wind can liberate the adsorbed gas, cooling the plasma and adding mass to the flow.

From our experience with the SSX prototype MHD wind tunnel, we estimate that five 3000 L-s^{-1} cryo pumps are required. The plasma volume will be about 400 times that of our prototype wind tunnel so we estimate that a minimum of 40–500 μF, 10 kV capacitors (25 kJ each, 1 MJ total) would be required. A weak (100 Gauss) axial field

https://doi.org/10.1017/S0022377815000227 Published online by Cambridge University Press

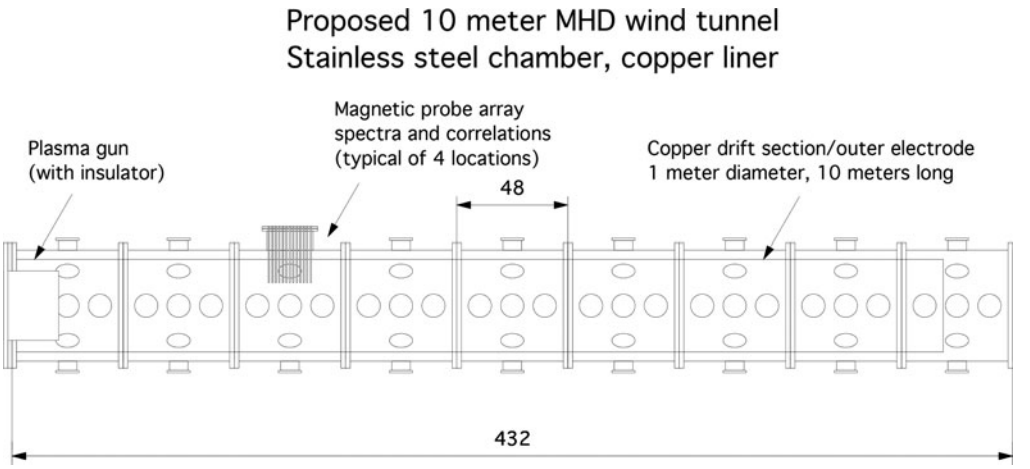


FIGURE 10. Preliminary design of 10 m MHD wind tunnel. The main vacuum chamber features nine 48-inch sections. The 10 m copper drift tube is placed inside.

would add some flexibility. Initial diagnostics would consist of a 100 magnetic probe array for high frequency fluctuation and correlation studies, a He–Ne interferometer system for density and density fluctuation studies, and ion Doppler spectroscopy for ion temperature studies.

Acknowledgements

This work was supported by grants from the Department of Energy (OFES), and the National Science Foundation (Physics Frontier Center for Magnetic Self Organization, CMSO). The authors gratefully acknowledge the assistance of technicians S. Palmer and P. Jacobs, and experimentalist students Adrian Wan '15, Peter Weck '15, Emily Hudson '17, Jeffrey Owusu-Boateng '16, Alexandra Werth '14, Darren Wienhold '12, Xingyu Zhang '12, Ken Flanagan '12, Bevan Gerber-Siff '10, Anna Phillips '10, Vernon Chaplin '07, and postdocs Tim Gray '01, Chris Cothran who all contributed to the SSX MHD wind tunnel.

REFERENCES

Alexandrova, O., Lacombe, C. and Mangeney, A. 2008 Spectra and anisotropy of magnetic fluctuations in the Earth's magnetosheath: cluster observations. *Ann. Geophys.* **26**, 3585.

Alexandrova, O., Saur, J., Lacombe, C., Mangeney, A., Mitchell, J., Schwartz, S. J. and Robert, P. 2009 Universality of solar-wind turbulent spectrum from MHD to electron scales. *Phys. Rev. Lett.* **103**, 165 003.

Batchelor, G. K. 1970 *Theory of Homogeneous Turbulence*. Cambridge, England: Cambridge University Press.

Bellan, P. M. 1979 Spontaneous, three-dimensional, constant-energy implosion of magnetic mirror fields. *Phys. Rev. Lett.* **43**, 858–861.

Bellan, P. M. 2000 *Spheromaks*. London, England: Imperial College Press.

Bickerton, R. J. 1997 Magnetic turbulence and the transport of energy and particles in tokamaks. *Plasma Phys. Control. Fusion* **39**, 339.

Binderbauer et al. 2010 Dynamic formation of a hot field reversed configuration with improved confinement by supersonic merging of two colliding high β compact toroids. *Phys. Rev. Lett.* **105**, 045 003.

Brown, M. R. 1997 Experimental evidence of rapid relaxation to large scale structures in turbulent fluids: selective decay and maximal entropy. *J. Plasma Phys.* **57**, 203.

https://doi.org/10.1017/S0022377815000227 Published online by Cambridge University Press

Brown, M. R. 1999 Experimental studies of magnetic reconnection. *Phys. Plasmas* **6**, 1717.

Brown, M. R., Cothran, C. D., Gray, T., Myers, C. E. and Belova, E. V. 2012 Spectroscopic observation of simultaneous bi-directional reconnection outflows in a laboratory plasma. *Phys. Plasmas* **19**, 080 704.

Bruno, R. and Carbone, V. 2013 The solar wind as a turbulence laboratory. *Living Rev. Sol. Phys.* **10**, 2. http://www.livingreviews.org/lrsp-2005-4

Buchenauer, C. J. and Jacobson, A. R. 1977 Quadrature interferometer for plasma density measurements. *Rev. Sci. Instrum.* **48**, 769–774.

Cothran, C. D., Brown, M. R., Gray, T., Schaffer, M. J. and Marklin, G. 2009 Observation of a helical self-organized state in a compact toroidal plasma. *Phys. Rev. Lett.* **103**, 215 002.

Cothran, C. D., Fung, J., Brown, M. R. and Schaffer, M. J. 2006 Fast, high resolution Echelle spectroscopy of a laboratory plasma. *Rev. Sci. Instrum.* **77**, 063 504.

Frisch, U. 1995 *Turbulence: The Legacy of A.N. Kolmogorov*. Cambridge, New York: Cambridge University Press.

Frisch, U., Pouquet, A., Leorat, J. and Mazure, A. 1975 Possibility of an inverse cascade of magnetic helicity in magnetohydrodynamic turbulence. *J. Fluid Mech.* **68**, 769–778.

Geddes, C. G. R., Kornack, T. W. and Brown, M. R. 1998 Scaling studies of spheromak formation and equilibrium. *Phys. Plasmas* **5**, 1027.

Gekelman, W. and Stenzel, R. 1984 *J. Geophys. Res.-Space Phys.* **89**, 2715.

Goldstein, M., Roberts, D. and Matthaeus, W. 1995 *Annu. Rev. Astron. Astrophys.* **33**, 283, ISSN 0066-4146.

Gray, T., Brown, M. R. and Dandurand, D. 2013 Observation of a relaxed plasma State in a quasi-infinite cylinder. *Phys. Rev. Lett.* **110**, 085 002.

Gray, T., Lukin, V. S., Brown, M. R. and Cothran, C. D. 2010 Three-dimensional reconnection and relaxation of merging spheromak plasmas. *Phys. Plasmas* **17**, 102 106.

Greco, A., Chuychai, P., Matthaeus, W. H., Servidio, S. and Dmitruk, P. 2008 Intermittent MHD structures and classical discontinuities. *Geophys. Res. Lett.* **35**, L19 111. doi:10.1029/2008GL035454.

Greco, A., Matthaeus, W. H., Servidio, S., Chuychai, P. and Dmitruk, P. 2009 Statistical analysis of discontinuities in solar wind ACE data and comparison with intermittent MHD turbulence. *Astrophys. J.* **691**, L111. doi:10.1088/0004-637X/691/2/L111.

Guo, H. et al. 2004 Flux conversion and evidence of relaxation in a high β plasma formed by high-speed injection into a mirror confinement structure. *Phys. Rev. Lett.* **92**, 245 001.

Hooper, E. B. et al. 2012 Sustained Spheromak Physics Experiment (SSPX): Design and physics results. *Plasma Phys. Control. Fusion* **54**, 113 001.

Hutchinson, I. H. 2002 *Principles of Plasma Diagnostics,* 2nd edn. Cambridge, England: Cambridge University Press.

Kolmogorov, A. N. 1941 The local structure of turbulence in incompressible viscous fluid for very large Reynolds numbers. *Dokl. Acad. Nauk. SSSR* **30**, 301.

Landreman, M., Cothran, C. D., Brown, M. R., Kostora, M. and Slough, J. T. 2003 Rapid multiplexed data acquisition: application to three-dimensional magnetic field measurements in a turbulent laboratory plasma. *Rev. Sci. Instrum.* **74**, 2361.

Lee, E., Brachet, M. E., Pouquet, A., Mininni, P. D. and Rosenberg, D. 2010 Lack of universality in de- caying magnetohydrodynamic turbulence. *Phys. Rev.* E **81**(1), 016 318.

Matthaeus, W. H. and Montgomery, D. 1980 *Ann. N.Y. Acad. Sci.* **357**, 203.

Matthaeus, W. H. and Velli, M. 2011 Who needs turbulence. *Space Sci. Rev.* **160**, 145.

Nornberg, M. D., Spence, E. J., Kendrick, R. D., Jacobson, C. M. and Forest, C. B. 2006 Measurements of the magnetic field induced by a turbulent flow of liquid metal. *Phys. Plasmas* **13**, 055 901.

Pouquet, A., Frisch, U. and Leorat, J. 1976 Strong MHD helical turbulence and nonlinear dynamo effect. *J. Fluid Mech.* **77**, 321–354.

Ren, Y., Almagri, A. F., Fiksel, G., Prager, S. C., Sarff, J. S. and Terry, P. W. 2011 *Phys. Rev. Lett.* **107**, 195 002.

Roberts, D. A. 2010 Evolution of the spectrum of solar wind velocity fluctuations from 0.3 to 5AU. *J. Geophys. Res.* **115**, A121 101.

https://doi.org/10.1017/S0022377815000227 Published online by Cambridge University Press

Sahraoui, F., Belmont, G., Rezeau, L., Cornilleau-Wehrin, N., Pincon, J. L. and Balogh, A. 2006 Anistropic turbulent spectra in the terrestrial magnetosheath as seen by the cluster spacecraft. *Phys. Rev. Lett.* **96**, 075 002.

Sahraoui, F., Goldstein, M., Robert, P. and Khotyaintsev, Y. 2009 Evidence of a cascade and dissipation of solar-wind turbulence at the electron gyroscale. *Phys. Rev. Lett.* **102**(23), 231 102.

Schaffner, D. A., Brown, M. R. and Lukin, V. S. 2014c Temporal and spatial turbulent spectra of MHD plasma and an observation of variance Anisotropy. *Astrophys. J.* **790**, 126.

Schaffner, D. A. Lukin, V. S., Wan, A. and Brown, M. R. 2014a Turbulence analysis of an experimental flux rope plasma. *Plasma Phys. Contol. Fusion* **56**, 064 003.

Schaffner, D. A., Wan, A., and Brown, M. R. 2014b Observation of turbulent intermittency scaling with magnetic helicity in an MHD plasma wind tunnel. *Phys. Rev. Lett.* **112**, 165 001.

Servidio, S., Matthaeus, W. H. and Dmitruk, P. 2008 Depression of nonlinearity in decaying isotropic MHD turbulence. *Phys. Rev. Lett.* **100**, 095 005. doi:10.1103 Phys. Rev. Lett.100.095005.

Servidio, S. et al. 2011a Magnetic reconnection as an element of turbulence. *Nonlinear Process. Geophys.* **18**, 675.

Servidio, S. et al. 2011b Statistical association of discontinuities and reconnection in magnetohydrodynamic turbulence. *J. Geophys. Res.* **116**, A09 102.

Taylor, J. B. 1974 Relaxation of Torodial Plasma and Generation of Reverse Magnetic Fields. *Phys. Rev. Lett.* **33**, 1139.

Tsurutani, B. T. and Smith, E. J. 1979 Interplanetary discontinuities - Temporal variations and the radial gradient from 1 to 8.5 AU. *J. Geophys. Res.* **84**, 2773.

Turner, W. et al. 1983 Investigations of the magnetic structure and the decay of a plasma gun generated compact torus. *Phys. Fluids* **26**, 1965.

Yordanova, E., Vaivads, A., Andre, M., Buchert, S. C. and Voros, Z. 2008 Magnetosheath plasma turbulence and its spatiotemporal evolution as observed by the cluster spacecraft. *Phys. Rev. Lett.* **100**, 205 003.

Zhang, X., Dandurand, D., Gray, T., Brown, M. R., and Lukin, V. S. 2011 Calibrated cylindrical mach probe in a plasma wind tunnel. *Rev. Sci. Instrum.* **82**, 033 510.

https://doi.org/10.1017/S0022377815000227 Published online by Cambridge University Press